Shear flow, phase change and matched asymptotic expansions: Pattern formation in mushy layers

Jerome A. Neufeld [a,b], J.S. Wettlaufer [b,c,d,*]

[a] *Institute of Theoretical Geophysics, Department of Applied Mathematics and Theoretical Physics, University of Cambridge, CMS Wilberforce Road, Cambridge, CB3 0WA, UK*

[b] *Department of Geology & Geophysics, Yale University, New Haven, CT, 06520, USA*

[c] *Department of Physics, Yale University, New Haven, CT, 06520, USA*

[d] *Program in Applied Mathematics, Yale University, New Haven, CT, 06520, USA*

ARTICLE INFO

ABSTRACT

In many scientific and engineering problems the solidification of an alloy leads to a highly convoluted crystalline matrix modeled as a thermodynamically controlled reactive porous medium called a *mushy layer*. We analyze the interaction of an external shear flow with a solidifying mushy layer through a corrugated mush–liquid interface. We find that the external flow can drive forced convective motions within the mushy layer resulting in the formation of a pattern of dissolution and solidification features transverse to the overall flow. Here we seek to lay bare the underlying processes through a systematic comparison of matched asymptotic expansions and numerical solutions. The success of our modeling effort draws substantially upon understanding gleaned from the fluid mechanics of boundary layers and the theory of multi-component solidification. The results have a broad range of implications in geophysics and materials science.

1. Introduction

The solidification of multi-component alloys is prevalent in a host of natural and industrial settings and gives rise to a striking array of solid forms and mixed phase products. At the growth rates typical of most environmental and industrial processes, the instability of a planar solid–liquid interface leads to a highly convoluted, dendritic interface between the solid and the liquid. The material that results is a reactive porous medium called a *mushy layer* in which the crystalline array is bathed in a multicomponent fluid. These systems are described by homogenizing conservation laws on a length scale much larger than the inter-dendrite spacing but much smaller than the size of the system [1].

Solidification of a mushy layer can be dramatically affected by both natural and forced motion within the array of crystals and the fluid from which it forms. Hence, mushy layers provide a rich setting in which to study the coupling of fluid dynamics and phase change. In particular, the form and structure of hydrodynamic boundary layers is coupled to moving phase boundaries, providing an ideal test bed for a number of general ideas including singular perturbation theory, matched asymptotic expansions, morphological stability and pattern formation.

There are many environmental and industrial phenomena for which the modeling approach we employ is applicable [1]. These include the freezing of polar oceans [2], the growth of the inner core of the Earth [3], and the structure of industrial materials [4]. In such circumstances intrinsic buoyancy induced flows and any externally imposed, or forced, flows have an essential influence on the growth process and the structure of the material. For example, when polar oceans freeze the ice formed is nearly pure, with the salt rejected forming a dense interstitial brine. This dense interstitial brine is unstable to convective motion. Indeed, field observations of warm sea ice in the presence of strong tidal currents ($\sim$0.17 m s^{-1}) show evidence for flow-induced desalination events [5]. Moreover, sea ice can move rapidly relative to the underlying ocean driving a shear flow [6,7] which can produce fluid motion within the sea ice itself. In any mushy layer the constraint of thermodynamic equilibrium results in phase change. Hence, fluid motions, both natural and forced, have controlling influences on the thermodynamic and mechanical properties of sea ice and the concentration and temperature of the ocean underneath. Motivated by the freezing of pipes, Gilpin et al. [8] studied the influence of an external shear flow on the evolution of a thick layer of ice. They observed an instability of the phase boundary in which a travelling wave of amplitude $\sim$1 cm and wavelength $\sim$10 cm grew over a time of order hours creating a large scale corrugation. Under

* Corresponding address: Yale University, 210 Whitney Avenue, New Haven, CT, 06520, USA.
    E-mail addresses: j.neufeld@damtp.cam.ac.uk (J.A. Neufeld), john.wettlaufer@yale.edu (J.S. Wettlaufer).

conditions satisfying the laboratory constraints evidence for this process was found in naturally occurring sea ice [9] and the associated increase in roughness influenced the heat flux across the ocean–ice interface. Finally, given these and other general influences of fluid flows on the material properties of mushy layers it is clear that the engineer may desire to tailor the properties of an end product using controlled fluid flows [4].

The circumstances just described comprise a subset of those that motivate the general study of the solidification of a binary alloy in the presence of an externally applied shear flow. Here, we examine the coupling between the external fluid and the solidification process through a corrugated mush–liquid interface. We begin by presenting the equations governing the evolution of both the mushy layer and the external fluid with prescribed far-field velocity, and review the constant growth rate steady state. Perturbations to the mush–liquid interface, which effectively couples flow within the external fluid to the thermodynamics of a solidifying mushy layer, are then considered using the following idealized analysis. Recognizing that the permeability of the mushy layer is typically small, we first consider the form of pressure perturbations at the mush–liquid interface generated by shear flow over the corrugated interface. The magnitude of pressure perturbations can be found using a Frobenius series approach [10] and is the result of the interaction between an outer inviscid flow and an inner viscous sublayer which we examine using matched asymptotics. These pressure perturbations drive a forced mode of convection within the mushy layer, and in so doing alter the local properties of the dendritic medium. We find an analytic expression for the critical porous medium Rayleigh number, which characterizes buoyant convection, as a function of the magnitude of the external flow speed in the limit where the latent heat released at the interface is large (characterized by large dimensionless Stefan number). This prediction of the onset and planform of the resultant local dissolution of the crystalline mushy layer informs models of solidification in the natural and technological settings discussed previously.

2. The governing equations

We model the solidification of a binary alloy coupled to an externally applied shear flow through a corrugated mush–liquid interface. While our study rests upon the framework and results of several previous numerical and experimental studies of such systems [10–13] in order to make this paper reasonably self contained, we review the basis of the formulation and relevant solutions of the system. This study is a reduced version of the forced system investigated numerically by us previously [10]. The asymptotic analysis described here marries classical work on the hydrodynamic stability of boundary layers [14] with the convective instability of mushy layers [1].

We consider an "ideal" mushy layer, composed of crystals of nearly pure solid grown at constant speed V into a uniform external shear flow of far-field velocity U_∞. In such ideal mushy layers the temperature and concentration of the mushy layer are coupled through the solutally dependent freezing point and any differences in density, diffusivity and specific heat between the liquid and solid are neglected (see reviews in [1,15]). Cooling the binary solution from below results in a mushy layer in the region $0 < z < \zeta$ that is bounded from below by solid and above by a semi-infinite liquid solution. The cold side, or in the geometry studied here the base, of the mushy layer is at the eutectic temperature T_E, the point at which a solid solution is formed. We note that these models apply equally well to mushy layers grown from super- and sub-eutectic concentrations, from above or from below. This is especially important as the forced mode is always active, while the presence of natural buoyant convection due to thermal or

compositional variations depends on bulk composition and the orientation with respect to gravity [16]. Due to the large interfacial surface area of the highly dendritic crystals comprising the mushy layer, two phase coexistence is rapidly reached and hence local thermodynamic equilibrium is assumed. Therefore, within the mushy layer the temperature T is related to the super-eutectic solute concentration C through a linear liquidus relationship; $T_L(C) = T_E + \Gamma(C - C_E)$ where Γ is the slope of the liquidus curve (constant over the range of relevance to our work) and C_E is the eutectic concentration. Far from the mush–liquid interface, the temperature in the overlying liquid tends to the far-field value T_∞. This is often the case in industrial settings where the application of external flows may be used to tailor material properties [4], but is unlikely to be satisfied over long periods in the growth of sea ice.

A principal motivation of our work concerns the mechanisms controlling the patterns of solidification and dissolution within the mushy layer which result from the confluence of buoyant and forced fluid motion. It has been shown that convective motions arising solely in the liquid due to the compositional boundary layer generate negligible flow within the mushy layer and have only a small effect on the morphology of the underlying material [10,15]. Thus, the essential mechanisms can be studied by neglecting several effects; the thermal and compositional contributions to buoyancy in the overlying liquid and the diffusion of solute within the mushy layer and the overlying liquid.

The governing equations for a mushy layer exposed to a shear flow were first developed by Feltham and Worster [11]. Here we include the effects of buoyancy within the crystal matrix to illustrate the progression from buoyancy to shear driven instability as the strength of the external flow is increased. Velocity, length, time and pressure are scaled by $V, \kappa/V, \kappa/V^2$ and ρV^2 respectively, where κ is the thermal diffusivity, and ρ the reference density. We make the Boussinesq approximation, that solid and liquid densities are everywhere equal save where they multiply gravity. The non-dimensional equations expressing conservation of heat and solute within the mushy layer can be written as

$$(\partial_t - \partial_z)(\theta - \mathcal{S}\phi) + \mathbf{u} \cdot \nabla\theta = \nabla^2\theta \quad \text{and} \tag{1}$$

$$(\partial_t - \partial_z)[(1 - \phi)\theta + \mathcal{C}\phi] + \mathbf{u} \cdot \nabla\theta = 0. \tag{2}$$

Here θ is the dimensionless temperature and concentration defined by

$$\theta = \frac{T - T_L(C_0)}{\Delta T} = \frac{C - C_0}{\Delta C}, \tag{3}$$

where $\Delta T = T_L(C_0) - T_E$, $\Delta C = C_0 - C_E$, ϕ is the volume fraction and $\mathbf{u}$ is the fluid velocity field. Two central dimensionless parameters characterize the thermodynamic properties of a mushy layer. The release of latent heat upon solidification is described by the Stefan number

$$\mathcal{S} = \frac{L}{c\Delta T}, \tag{4}$$

where L is the latent heat of fusion and c is the specific heat capacity. The rejection of solute is captured by the composition ratio

$$\mathcal{C} = \frac{C_S - C_0}{C_0 - C_E}, \tag{5}$$

where C_S is the concentration of the solid.

Importantly, the mushy layer is treated as a porous medium using Darcy's law,

$$\mathbf{u} = -\frac{\Pi_0}{Pr}\nabla p - R_m\theta\hat{\mathbf{z}}, \tag{6}$$

written here in non-dimensional form where p is the dynamic pressure, $Pr = \nu/\kappa$ is the Prandtl number which is the ratio of

kinematic viscosity, ν, to thermal diffusivity, and the dimensional average permeability of the mushy layer, $\tilde{\Pi}_0$, is characterized by the non-dimensional Darcy number

$$\Pi_0 = \frac{\tilde{\Pi}_0}{(\kappa/V)^2}. \tag{7}$$

In contrast to [11], the effects of both thermal and compositional buoyancy are incorporated through a porous medium Rayleigh number

$$R_m = \frac{g(\beta - \Gamma\alpha)\Delta C\tilde{\Pi}_0(\kappa/V)}{\kappa\nu}. \tag{8}$$

Here g is the acceleration due to gravity, and α and β are the thermal and solutal coefficients of expansion respectively. In general, through the solid fraction, the permeability of the mushy layer is anisotropic and depth dependent, but we simplify the analysis substantially by considering a locally isotropic dimensional permeability $\tilde{\Pi}_0$ which is, to leading order, constant with depth. The permeability used in the following theoretical analysis is therefore best envisaged as a depth-averaged permeability.

Within the overlying liquid advection and diffusion of heat are modeled by

$$(\partial_t - \partial_z)\theta + \mathbf{u} \cdot \nabla\theta = \nabla^2\theta, \tag{9}$$

and flow within the incompressible liquid is governed by the Navier–Stokes equations

$$(\partial_t - \partial_z)\mathbf{u} + \mathbf{u} \cdot \nabla\mathbf{u} = -\nabla p + Pr\nabla^2\mathbf{u}, \tag{10}$$

with conservation of mass given as

$$\nabla \cdot \mathbf{u} = 0. \tag{11}$$

The following thermodynamic boundary conditions are imposed;

$$\theta = -1 \quad \text{at } (z = 0), \tag{12a}$$

$$\theta = 0, \tag{12b}$$

$$\phi = 0, \tag{12c}$$

$$[\theta]_l^m = 0, \tag{12d}$$

$$\phi\mathcal{S}(1 + v_n) = [\hat{\mathbf{n}} \cdot \nabla\theta]_l^m \quad \text{at } (z = \zeta), \tag{12e}$$

and $\quad \theta \to \theta_\infty \quad \text{at } (z \to \infty). \tag{12f}$

Here $\theta_\infty = [T_\infty - T_L(C_0)]/\Delta T$ is the dimensionless far-field temperature, $\hat{\mathbf{n}}$ is the unit normal pointing into the melt, v_n is the normal growth velocity of the interface and $[\ ]_l^m$ denotes a jump in the quantities across the mush–liquid interface. These boundary conditions express the following physical concepts. The base of the mushy layer is fixed at the eutectic temperature (12a) and, owing to the neglect of compositional diffusion within the liquid, the mush–liquid interface is fixed at the liquidus temperature of the bulk concentration (12b). The requirement of zero solid fraction at the mush–liquid interface (12c) follows from the hypothesis of marginal equilibrium [1,17]. We require continuity of both the thermal field (12d) and conservation of thermal energy at the mush–liquid interface (12e), commonly called the Stefan condition. Finally, the temperature in the overlying liquid asymptotes to its far-field value (12f).

The boundary conditions on the fluid velocity are;

$$w = 0 \quad \text{at } (z = 0), \tag{13a}$$

$$[\mathbf{u} \cdot \hat{\mathbf{n}}]_l^m = 0, \tag{13b}$$

$$[p]_l^m = 0, \tag{13c}$$

$$[\mathbf{u} \times \hat{\mathbf{n}}]_l = 0 \quad \text{at } (z = \zeta), \tag{13d}$$

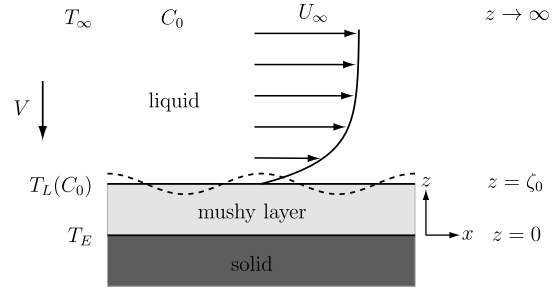and $\quad \mathbf{u} \to U_\infty\hat{\mathbf{x}} \quad \text{at } (z \to \infty), \tag{13e}$

Fig. 1. Illustration of a shear flow over a mushy layer growing at constant rate V. Flow is coupled through a perturbed mush–liquid interface indicated by the dotted line. We depict the metallurgically relevant geometry of solidification from below, but note that the analysis of solidification from above proceeds in an identical manner.

where U_∞ is the imposed far-field velocity. Condition (13a) imposes vanishing velocity at the base of the mushy layer. At the mush–liquid interface (13b) and (13c) express continuity of mass flux and pressure respectively. In the limit of small mushy layer permeability we use a no-slip condition at the mush–liquid interface (13d) rather than the more general Beavers–Joseph boundary condition [18]. Finally, we require the velocity within the liquid to asymptote to its far-field value (13e).

2.1. Basic steady-state solution

The steady-state solution to this system was found by Feltham and Worster [11] in the limit $\mathcal{C} \gg 1$, and is shown schematically in Fig. 2. We denote this solution, describing a stagnant mushy layer ($\mathbf{u}_0^m = 0$), by a subscript zero. The steady growth of the mushy layer produces an asymptotic suction profile in the overlying liquid

$$\mathbf{u}_0^l = (u_0^l, v_0^l, w_0^l)$$

$$= (U_\infty[1 - e^{-(z-\zeta_0)/Pr}], 0, 0), \tag{14}$$

where the $\hat{\mathbf{x}}$ coordinate is oriented with the flow as shown in Fig. 1. The temperature in the overlying liquid decays to its far-field value,

$$\theta_0^l = \theta_\infty[1 - e^{-(z-\zeta_0)}], \tag{15}$$

and the temperature and solid fraction of the mushy layer are given by

$$\theta_0^m = \frac{\theta_\infty}{\Lambda}[1 - e^{-\Lambda(z-\zeta_0)}] \quad \text{and} \tag{16}$$

$$\phi_0^m = -\frac{\theta_0^m}{\mathcal{C}}, \tag{17}$$

where $\Lambda = 1 + \mathcal{S}/\mathcal{C}$. Finally, the depth of the mushy layer, as determined by the Stefan condition (12e), is given by

$$\zeta_0 = \frac{1}{\Lambda} \ln\left[1 + \frac{\Lambda}{\theta_\infty}\right]. \tag{18}$$

3. Perturbations to forced flow in the liquid

Natural convective motions both within, and external to, solidifying crystalline arrays are driven by gradients in the temperature and concentration of the interstitial and ambient fluid respectively. Here we focus on convective motions within the mushy layer forced by an external shear flow interacting with a corrugated mush–liquid interface. During the development of this work we discovered that an external flow can have a pronounced effect on the stability of these natural convective modes, and can lead to new forced convective modes which arise from the coupling
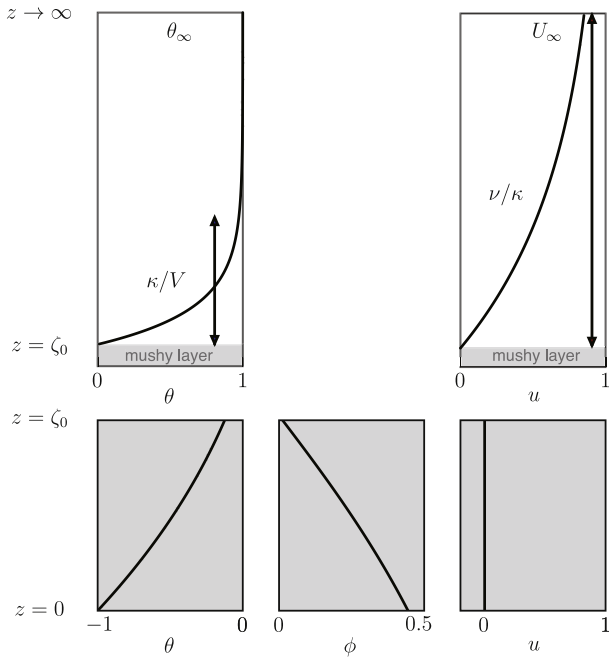
Fig. 2. A schematic of the base-state thermal field θ and horizontal velocity u within the overlying liquid, and the base-state thermal field θ, solid fraction ϕ and horizontal velocity u within the mushy layer. The length scales of the thermal and viscous boundary layers in the external liquid are indicated.

of the external flow and a corrugated mush–liquid interface. A simple model of this coupling can be found by considering only perturbations to the external fluid velocity in the overlying liquid, neglecting variations in temperature and concentration. In this limit, a standard normal mode analysis can be posed, and the resultant equation governing perturbations to the flow field in the liquid is a modified Orr–Sommerfeld equation of the form

$$[Pr(D^2 - k^2) + D][D^2 - k^2]w_1$$
$$= ikU_\infty[(1 - e^{-(z-\zeta_0)/Pr})(D^2 - k^2) - Pr^{-2}e^{-(z-\zeta_0)/Pr}]w_1, \quad (19)$$

with boundary conditions

$$w_1 = 0, \quad Dw_1 = ik\zeta_1 \frac{U_\infty}{Pr}, \quad (z = \zeta_0) \quad (20)$$

and $\quad w_1 \to 0, \quad Dw_1 \to 0, \quad (z \to \infty) \quad (21)$

where $D \equiv d/dz$. The Orr–Sommerfeld problem (19) with boundary conditions (20) and (21) has been previously solved numerically using a Frobenius series method [12] which we review for comparison with the asymptotic analysis performed here.

The problem is greatly simplified by first using the transformation $s = e^{-(z-\zeta_0)/Pr}$ and writing $\alpha = kPr$. Finally, we recognize that a natural small parameter exists for this system, $\epsilon \equiv (i\alpha U_\infty)^{-1}$, since the magnitude of the external shear flow can be much larger than typical growth velocities, $U_\infty \gg 1$. The resulting transformation of (19) along with the associated boundary conditions were solved using a Frobenius series of the form

$$w_1 = \lambda_1 s^{r_1} \sum_{j=0}^{\infty} a_j s^j + \lambda_2 s^{r_2} \sum_{j=0}^{\infty} b_j s^j. \quad (22)$$

The roots of the resultant indicial equation, which ensure that the solution remains bounded as $z \to \infty$ and $s \to 0$, are given by

$$r_1 = \alpha \quad \text{and} \quad (23a)$$

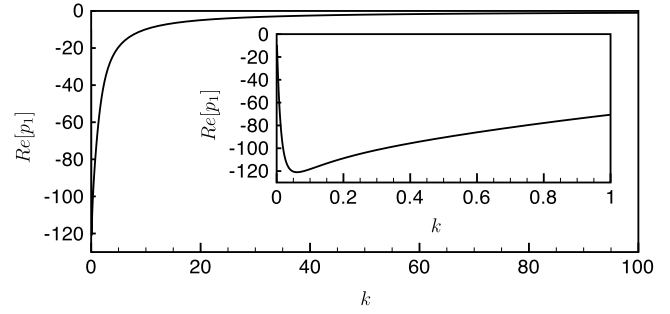$$r_2 = \frac{1}{2}[1 - \sqrt{1 + 4\alpha(\alpha + \epsilon^{-1})}], \quad (23b)$$

Fig. 3. Real component of the pressure perturbation at the mush–liquid interface for $U_\infty = 100$ and $Pr = 10$. Note that the maximum pressure perturbation is $Re[p_1] \simeq -121$ at $k \simeq 0.06$ which corresponds to a negative pressure perturbation at the peaks of the interfacial deflection. The inset shows the pressure perturbation over the range $k = [0, 1]$.

and coefficients a_j and b_j are obtained from the recurrence relation

$$[(j + r)^2 - \alpha^2][(j + r)^2 - (j + r) - \alpha^2 - \epsilon^{-1}]a_j$$
$$= \epsilon^{-1}[\alpha^2 + 1 - (j + r - 1)^2]a_{j-1}, \quad (24)$$

with $a_0 = b_0 = 1$. The constants λ_1 and λ_2 are then found by applying the boundary conditions (20) on the perturbed mush–liquid interface

$$\lambda_1 = \frac{-\epsilon^{-1}/Pr}{\sum_{j=0}^{\infty}(r_2 + j)a_j - \beta\sum_{j=0}^{\infty}(r_4 + j)b_j} \quad \text{and} \quad (25a)$$

$$\lambda_2 = -\beta\lambda_1, \quad (25b)$$

with

$$\beta = \sum_{j=0}^{\infty} a_j \Big/ \sum_{j=0}^{\infty} b_j. \quad (26)$$

Thus, the solution to the perturbed velocities in the liquid allows the pressure perturbation felt at the mush–liquid interface to be evaluated as

$$p_1 = \frac{-(D_s^2 - \alpha^2)D_s w_1 + D_s^2 w_1}{\alpha^2}, \quad (27)$$

where $D_s \equiv d/ds$.

A typical example of the real component of the pressure perturbation is shown in Fig. 3 for $U_\infty = 100$ and $Pr = 10$. However, we neglect the imaginary component since this leads only to a translation of the interface. We see that the maximal pressure perturbation occurs at $k = 0.06$. It is apparent that as $k \to \infty$, $Re[p_1] \to 0^-$, and that as $k \to \infty$, $Re[p_1] \sim -kU_\infty^2/Pr$. This pressure perturbation can be interpreted as a Bernoulli suction effect; shear flow over the perturbed mush–liquid interface leads to *negative* pressure perturbations at the *peaks* and *positive* pressure perturbations at the *troughs*. We can couple these pressure perturbations to the dynamics of the mushy layer to provide a quasi-analytical approach to understanding the effect of an external flow on convection in the mushy layer. Clearly, the large and small wavenumber limits provide strong motivation for an analytic study of the perturbed flow field within the liquid.

4. Matched asymptotic approach to perturbed flow in the liquid

Flow over an undulating, or corrugated, boundary has been studied previously by a number of authors [19–21, e.g.,]. Benjamin [19] used a perturbed coordinate system to calculate the normal and tangential stresses on a corrugated boundary in the presence

of an applied flow. Charru et al. [20,21] extended this analysis and found analytic solutions for the perturbed velocities associated with Poiseuille flow over a corrugated boundary.

Many of these mathematical models bear a striking similarity to related work on the hydrodynamic stability of shear flows, as reviewed by Reid [22] and by Drazin and Reid [14] in their comprehensive book. Of particular relevance to this analysis are the studies of the hydrodynamic stability of the asymptotic suction profile by Hughes and Reid [23], Hocking [24] and Lakin and Reid [25].

Numerical solution of the full perturbation equations describing forced convection in the solidifying mushy layer system reveals that convection is forced only at large external velocities, $U_\infty \gg 1$. We note that the small parameter ϵ, which is inversely proportional to U_∞, multiplies the highest derivative and is therefore a singular perturbation. This results in the expected viscous boundary layer at the mush–liquid interface. As is typical for this type of system, an inner and an outer solution are found. The inner solution describes the velocity perturbations in the inner boundary layer where the effects of viscosity are strongly felt, and the outer solution describes the region where, to leading order, the flow is inviscid. These solutions are then matched in an intermediate region and it is these matched solutions that are used to derive the pressure perturbations at the mush–liquid boundary.

4.1. Outer solution

We first examine the outer approximations to the Orr–Sommerfeld equation developed along standard lines [14]. These can be characterized as a set of outer 'inviscid' solutions which can be readily obtained from an expansion of w_1 in ϵ. The second of these, termed the outer 'viscous' solution is sought within the framework of a WKB approximation [26].

4.1.1. Outer 'inviscid' solution

Following the analysis developed by Drazin and Reid [14] we first examine the outer approximations to the Orr–Sommerfeld equation. In taking the limit of (19) as $\epsilon \to 0$ Rayleigh's stability equation is obtained. Solutions to Rayleigh's stability equation were first formulated by Tollmien [27] as

$$\tilde{w}_1^{(0)} = z P_A(z) \tag{28}$$

and $\quad \tilde{w}_2^{(0)} = P_B(z) + z \ln(z) P_A(z), \tag{29}$

where both $P_A(z)$ and $P_B(z)$ are power series in z with leading order terms of unity. The approach proceeds by expanding the outer solution as

$$w = \sum_{n=0}^{\infty} \epsilon^n \tilde{w}^{(n)}. \tag{30}$$

The resulting perturbation equations at $\mathcal{O}(\epsilon^0)$ and $\mathcal{O}(\epsilon^1)$ are

$$(1 - e^{-z})(D^2 - \alpha^2)\tilde{w}^{(0)} + e^{-z}\tilde{w}^{(0)} = 0, \tag{31}$$

$$[(D^2 - \alpha^2)^2 + D(D^2 - \alpha^2)]\tilde{w}^{(1)}$$
$$= [(1 - e^{-z})(D^2 - \alpha^2) + e^{-z}]\tilde{w}^{(1)}, \tag{32}$$

respectively.

Solutions can be determined analytically from the steady-state asymptotic suction profile as follows. First, $\tilde{w}^{(0)}(z)$ is defined as $\tilde{w}^{(0)}(z) = e^{-\alpha z} f(s)$, where $s = e^{-z}$, and therefore Eq. (31) becomes the hypergeometric equation [23]

$$(1 - s)s D_s^2 f + (1 + 2\alpha)(1 - s)D_s f + f = 0. \tag{33}$$

Therefore, to $\mathcal{O}(\epsilon^0)$

$$\tilde{w}_1^{(0)} + \tilde{w}_2^{(0)} \equiv \tilde{w}_{1+2}^{(0)}(z)$$
$$= a e^{-\alpha z} {}_2F_1(\alpha + \sqrt{1 + \alpha^2}, \alpha$$
$$\quad - \sqrt{1 + \alpha^2}, 1 + 2\alpha; e^{-z})$$
$$\quad + b e^{\alpha z} {}_2F_1(-\alpha + \sqrt{1 + \alpha^2},$$
$$\quad - \alpha - \sqrt{1 + \alpha^2}, 1 - 2\alpha; e^{-z}), \tag{34}$$

where a and b are constants, and ${}_2F_1(a, b, c; y)$ is the hypergeometric function. Because the solution must remain bounded as $z \to \infty$ we require that $b = 0$. The remaining component of the solution is then normalized at $z = 0$, giving $a = {}_2F_1(\alpha + \sqrt{1 + \alpha^2}, \alpha - \sqrt{1 + \alpha^2}, 1 + 2\alpha; 1)^{-1}$. For more compact notation we define $p = \alpha + \sqrt{1 + \alpha^2}$ and $q = \alpha - \sqrt{1 + \alpha^2}$, and thus the outer inviscid solution is found to be

$$\tilde{w}_{1+2}^{(0)} = e^{-\alpha z} \frac{{}_2F_1(p, q, 1 + p + q; e^{-z})}{{}_2F_1(p, q, 1 + p + q; 1)}$$
$$= \frac{e^{-\alpha z}}{{}_2F_1(p, q, 1 + p + q; 1)} \sum_{n=0}^{\infty} \frac{(p)_n (q)_n}{(1 + p + q)_n} \frac{e^{-nz}}{n!}, \tag{35}$$

where $(y)_n \equiv \Gamma(y + n)/\Gamma(y)$ denotes the Pochhammer symbol, and $\Gamma(n + 1) = n!$ is the Gamma function with integer argument. To facilitate matching with the inner solutions the following linear transformation of the hypergeometric function found in [28] is useful;

$$\frac{{}_2F_1(p, q, 1 + p + q; e^{-z})}{{}_2F_1(p, q, 1 + p + q; 1)}$$
$$= 1 - (1 - e^{-z}) \ln(1 - e^{-z}) {}_2F_1(1 + p, 1 + q, 2; 1 - e^{-z})$$
$$\quad - \sum_{n=0}^{\infty} A_n \frac{(1 - e^{-z})^{n+1}}{(n + 1)!}, \tag{36}$$

where the coefficients A_n are defined as

$$A_n = \frac{\Gamma(1 + p + n)\Gamma(1 + q + n)}{\Gamma(1 + p)\Gamma(1 + q)\Gamma(n + 1)}$$
$$\quad \times \{\psi(1 + p + n) + \psi(1 + q + n)$$
$$\quad - \psi(n + 1) - \psi(n + 2)\}, \tag{37}$$

and $\psi(n) = \Gamma'(n)/\Gamma(n)$ is the digamma function. Thus, as $z \to 0$ solutions of the outer equation can be written in the form

$$\tilde{w}_{12}^{(0)}(z) = (1 - \alpha z)(1 - z \ln z - A_0 z). \tag{38}$$

Note that in the special case of the asymptotic suction profile the power series first introduced by Tollmien [27] can be solved analytically as displayed through the series definition of the hypergeometric function found in the solution for $\tilde{w}^{(0)}(z)$.

4.1.2. Outer 'viscous' solution

The WKB method of analyzing Eq. (19) not only reproduces the inviscid hypergeometric solution, but also provides a 'viscous' outer solution to the governing equations. We thus proceed by substituting

$$w_1(z) = \exp\left[\epsilon^{-1/2} \sum_{n=0}^{\infty} \epsilon^{n/2} g_n(z)\right] \tag{39}$$

into (19) giving

$$(g_0')^4 = (1 - e^{-z})(g_0')^2, \tag{40}$$

to $\mathcal{O}(\epsilon^{-1})$ with solutions

$$g_0 = \text{constant} \quad \text{and} \quad g_0(z) = \pm \int_0^z \sqrt{1 - e^{-z}} \, dz. \tag{41}$$

Hence, to $\mathcal{O}(\epsilon^{-1/2})$, Eq. (19) becomes

$$- g_0''[6(g_0')^2 - (1 - e^{-z})]$$

$$= 2g_0'[2(g_0')^2 - (1 - e^{-z})](g_1') + (g_0')^3, \qquad (42)$$

which is satisfied identically for $g_0 = $ constant and for $g_0(z) = \int_0^z \sqrt{1 - e^{-t}} dt$ has solution

$$g_1(z) = -\frac{z}{2} + \ln(1 - e^{-z})^{-5/4}. \qquad (43)$$

Proceeding to $\mathcal{O}(\epsilon^{-1})$, using $g_0 = $ constant recovers the inviscid outer solution and, to $\mathcal{O}(\epsilon^{-1/2})$, the outer 'viscous' solution is

$$\tilde{w}_3^{(0)}(z) = \exp[-\epsilon^{-1/2} g_0(z) + g_1(z)], \qquad (44)$$

where a fourth solution $\tilde{w}_4^{(0)}(z)$ has been discarded because it is unbounded as $z \to \infty$.

4.2. Inner solution

To obtain the inner solution describing the viscous boundary layer near the mush–liquid interface we expand the vertical scale around $z = 0$ by setting

$$\xi = z/\epsilon^\ell,$$

where ℓ is an unknown stretching to be determined from the governing equation. In the case of arbitrary α the Orr–Sommerfeld equation is best reformulated in terms of the vorticity, $\tilde{\Omega}$, here defined as

$$(D_\xi^2 - \beta^2)\tilde{W} = \tilde{\Omega},$$

where $\beta = \epsilon^{1/3}\alpha$ is the rescaled wavenumber and $\tilde{W}$ is the vertical velocity in the inner region. By equating the resulting lowest-order terms in the Orr–Sommerfeld equation we find that

$$\epsilon^{-4\ell} D_\xi^2 \tilde{\Omega} = \epsilon^{-1+\ell-2\ell} \xi \tilde{\Omega},$$

from which we determine that $\ell = 1/3$. Therefore, the lowest order general solution for the perturbed vorticity is

$$\tilde{\Omega} = \mathcal{C}\text{Ai}(\xi) + \mathcal{D}\text{Bi}(\xi), \qquad (45)$$

where Ai and Bi are Airy functions. Because the vorticity must be constrained as $\xi \to \infty$ we must have $\mathcal{D} = 0$. Integrating the vorticity equation twice, to lowest order, we find that the vertical velocity is given by

$$\tilde{W}^{(0)} = \mathcal{A}e^{-\beta\xi} + \mathcal{B}e^{\beta\xi} + \frac{\mathcal{C}}{2\beta}\left\{ e^{-\beta\xi} \int_0^\xi e^{\beta t}\text{Ai}(t)dt \right.$$

$$\left. + e^{\beta\xi} \int_\xi^\infty e^{-\beta t}\text{Ai}(t)dt \right\}. \qquad (46)$$

This formula is most readily understood in two limits. In the large wavelength limit where both α and β are small, $e^{\pm\beta\xi} \simeq 1 \pm \beta\xi$, and so the velocity perturbations can be reformulated in terms of the three linearly independent solutions

$$\tilde{W}_1^{(0)}(\xi) = A, \qquad (47)$$

$$\tilde{W}_2^{(0)}(\xi) = B\xi, \qquad (48)$$

$$\text{and} \quad \tilde{W}_3^{(0)}(\xi) = C \int_\infty^\xi \int_\infty^t \text{Ai}(t') \, dt'dt, \qquad (49)$$

where A, B and C are convenient recombinations of the constants $\mathcal{A}$, $\mathcal{B}$ and $\mathcal{C}$ and are determined by matching to the outer solution.

In the small wavelength limit where α and β are large, perturbations in the fluid layer are confined to a narrow region immediately adjacent to the mush–liquid interface. In this limit, the inviscid outer solution is well approximated by

$$\tilde{w}_{1+2}^{(0)}(z) = e^{-\alpha z},$$

and so $\mathcal{B} \to 0$. The remaining constants can therefore be simply determined through application of the two boundary conditions at the mush–liquid interface.

4.3. Matching: large wavelength (small α) limit

4.3.1. Matching the 'inviscid' outer solution

Composite solutions are constructed by matching the inner and outer solutions. To this end, the inner limit of the outer solution $\tilde{w}_{12}^{(0)}$ is

$$\tilde{w}_{12}^{(0)} \sim (1 - \alpha z)(1 - z \ln z - A_0 z). \qquad (50)$$

Recalling the inner solutions $\tilde{W}_1^{(0)} = A$ and $\tilde{W}_2^{(0)} = B\xi$, we can determine the constants A and B by matching the inner limit of the outer solution to the outer limit of the inner solution yielding

$$A = 1 \qquad (51)$$

and $\quad B = -\epsilon^{1/3}(\alpha + A_0)$

$$= \epsilon^{1/3}[1 - 2\gamma - \alpha - \psi(1 + p) - \psi(1 + q)], \qquad (52)$$

where $\gamma = 0.5772$ is Euler's constant. The logarithmic term in (50), $z \ln z$, must be determined by matching with the inner solution at second order which is

$$\left(\frac{d^2}{d\xi^2} - \xi \right) \frac{d^2\tilde{W}^{(1)}}{d\xi^2} = \left(\frac{1}{2}\xi^2 - \frac{d^3}{d\xi^3} - 1 \right) \tilde{W}^{(0)}. \qquad (53)$$

Matching of the logarithmic term is achieved by considering only the term $\tilde{W}^{(0)} \sim 1$ in the second order inner equations, thus providing the solution

$$Q_3(\xi) \equiv \frac{d^2\tilde{W}_2^{(1)}}{d\xi^2}$$

$$= 2\pi e^{i\pi/6} \left\{ \text{Ai}(\xi) \int_\infty^\xi \text{Bi}(t)dt - \text{Bi}(\xi) \int_\infty^\xi \text{Ai}(t)dt \right\}.$$

Reid [22] showed that the asymptotic (large ξ) behavior of $Q_3(\xi)$ is

$$Q_3(\xi) \sim \frac{1}{\xi} + \mathcal{O}\left(\frac{1}{\xi^4} \right),$$

and integration of the function $Q_3(\xi)$ reveals the nature of this first order solution as

$$\tilde{W}_2^{(1)} = \int_\infty^\xi \int_\infty^t \left[Q_3(t') - \frac{1}{t'} \right] dt'dt + \xi \ln \xi + \mathcal{F}\xi + \mathcal{G}, \qquad (54)$$

which has an asymptotic behavior as $\xi \to \infty$ that is

$$\tilde{W}_2^{(1)} \sim \xi \ln \xi + \mathcal{F}\xi + \mathcal{G}. \qquad (55)$$

Matching this to the $z \ln z$ term in the inner limit of the outer solution gives the constants

$$\mathcal{G} = 0,$$

and $\quad \mathcal{F} = \ln \epsilon^{1/3},$

and (54) becomes

$$\tilde{W}_2^{(1)} = \int_\infty^\xi \int_\infty^t \left[Q_3(t') - \frac{1}{t'} \right] dt'dt + \xi \ln(\epsilon^{1/3}\xi). \qquad (56)$$

Finally, a composite solution is constructed using the additive rule of van Dyke [29] viz.,

$$w_{12}^{(0)} = \tilde{w}_{12}^{(0)} + \tilde{W}_1^{(0)} + \tilde{W}_2^{(0)} + \epsilon^{1/3}[\tilde{W}_1^{(1)} - \tilde{W}_2^{(1)}] - \text{common part},$$

providing the composite solution

$$\tilde{w}_{12} = e^{-\alpha z} \frac{_2F_1(p, q, 1 + p + q; e^{-z})}{_2F_1(p, q, 1 + p + q; 1)} - \epsilon^{1/3}\tilde{W}_2^{(1)} + z \ln z$$

$$= e^{-\alpha z} \frac{_2F_1(p, q, 1 + p + q; e^{-z})}{_2F_1(p, q, 1 + p + q; 1)}$$

$$- \epsilon^{1/3} \int_\infty^\xi \int_\infty^t \left[Q_3(t') - \frac{1}{t'} \right] dt'dt. \qquad (57)$$

4.3.2. Matching the 'viscous' outer solutions

The solutions $\tilde{w}_3^{(0)}$ and $\tilde{W}_3^{(0)}$ can be matched in the following way. Taking the inner limit of $\tilde{w}_3^{(0)}$ gives

$$\tilde{w}_3^{(0)} \sim z^{-5/4} \exp[-2/3\epsilon^{-1/2}z^{3/2}], \tag{58}$$

and the outer expansion of $\tilde{W}_3^{(0)}$ is given by

$$\int_\infty^\xi \int_\infty^t \mathrm{Ai}(t')\mathrm{d}t'\mathrm{d}t \sim \frac{C}{2\sqrt{\pi}}\xi^{-5/4}\exp[-2/3\xi^{3/2}]$$
$$= C\frac{\epsilon^{5/12}}{2\sqrt{\pi}}z^{-5/4}\exp[-2/3\epsilon^{-1/2}z^{3/2}], \tag{59}$$

where the last expression is written in terms of the outer variable. It is evident that in the overlapping region these two solutions are identical when

$$C = 2\sqrt{\pi}\epsilon^{-5/12}.$$

In this case, a composite solution is constructed using the multiplicative rule of van Dyke [29];

$$\text{composite} = \frac{(\text{inner}) \times (\text{outer})}{(\text{common part})},$$

which leads to

$$\tilde{w}_3 = \left(\frac{1-e^{-z}}{z}\right)^{-5/4}\exp\left[-\frac{z}{2} - \epsilon^{-1/2}\left\{g_0(z) - \frac{2}{3}z^{3/2}\right\}\right]$$
$$\times \int_\infty^\xi \int_\infty^t \mathrm{Ai}(t')\mathrm{d}t'\mathrm{d}t. \tag{60}$$

4.4. Asymptotic solution for perturbed vertical velocities

We construct an asymptotic solution for the perturbed vertical velocity using our composite solutions $\tilde{w}_{1+2}$ and $\tilde{w}_3$ as follows. The asymptotic solution is defined as

$$w_1 = a\tilde{w}_{1+2} + b\tilde{w}_3, \tag{61}$$

for which the application of the final boundary conditions

$$w_1(0) = 0 = a\tilde{w}_{1+2}(0) + b\tilde{w}_3(0),$$

and $\quad Dw_1(0) = \frac{\epsilon^{-1}}{Pr} = a\tilde{w}'_{1+2} + b\tilde{w}'_3,$

determine the constants

$$a = \frac{\epsilon^{-1}}{Pr}\frac{\tilde{w}_3(0)}{\tilde{w}_3(0)\tilde{w}'_{1+2}(0) - \tilde{w}_{1+2}(0)\tilde{w}'_3(0)}, \tag{62}$$

and $\quad b = -\frac{\epsilon^{-1}}{Pr}\frac{\tilde{w}_{1+2}(0)}{\tilde{w}_3(0)\tilde{w}'_{1+2}(0) - \tilde{w}_{1+2}(0)\tilde{w}'_3(0)}. \tag{63}$

Finally, we arrive at the asymptotic solution

$$w_1 = \frac{\epsilon^{-1}}{Pr}\frac{\tilde{w}_{1+2}(z)\tilde{w}_3(0) - \tilde{w}_3(z)\tilde{w}_{1+2}(0)}{\tilde{w}_3(0)\tilde{w}'_{1+2}(0) - \tilde{w}_{1+2}(0)\tilde{w}'_3(0)}, \tag{64}$$

which depends on the values of the composite parts evaluated at the origin.

4.4.1. Evaluating the composite solutions at the origin

Because the constants are obtained from the composite solutions evaluated at the origin, they take the value of the inner solution at $\xi = 0$ and are

$$\tilde{w}_{1+2}(0) = 1 - \epsilon^{1/3}\frac{2\pi}{\sqrt{3}}\frac{3^{-1/3}}{\Gamma(1/3)}e^{2\pi i/3}, \tag{65}$$

$$\tilde{w}'_{1+2}(0) = \frac{\pi i}{2} + \frac{\ln 3}{3} - \frac{4}{3}\gamma - \ln|\epsilon^{1/3}|$$
$$- \alpha - \psi(1+p) - \psi(1+q), \tag{66}$$

$$\tilde{w}_3(0) = 2\sqrt{\pi}\epsilon^{-5/12}\frac{3^{-1/3}}{\Gamma(1/3)}, \tag{67}$$

and $\quad \tilde{w}'_3(0) = -\frac{2\sqrt{\pi}}{3}\epsilon^{-3/4}. \tag{68}$

4.5. Matching: short wavelength (large α) limit

In the small wavelength ($\alpha \gg 1$) limit velocity perturbations in the liquid are confined to a narrow region adjacent to the mush–liquid interface. In this case, the outer solution is well approximated by

$$\tilde{w}_{1+2}^{(0)}(z) = ae^{-\alpha z}, \tag{69}$$

and the inner equation can be approximated by

$$\tilde{W}(\xi) = \mathcal{A}e^{-\beta\xi} + \frac{\mathcal{C}}{2\beta}\left\{e^{-\beta\xi}\int_0^\xi e^{\beta t}\mathrm{Ai}(t)\mathrm{d}t + e^{\beta\xi}\int_\xi^\infty e^{-\beta t}\mathrm{Ai}(t)\mathrm{d}t\right\}. \tag{70}$$

The constants are readily obtained through application of the remaining boundary conditions at the mush–liquid interface, and are

$$\mathcal{A} = \frac{\epsilon^{-1}}{2\alpha Pr} \tag{71}$$

and $\quad \mathcal{C} = \frac{\epsilon^{-2/3}}{Pr}\left(\int_0^\infty e^{-\beta t}\mathrm{Ai}(t)\mathrm{d}t\right)^{-1}. \tag{72}$

Therefore, the velocity perturbations are given by

$$\tilde{w}(z) = \frac{\epsilon^{-1}}{2\alpha Pr}\left\{e^{-\alpha z} + \frac{e^{-\alpha z}\int_0^\xi e^{\beta t}\mathrm{Ai}(t)\mathrm{d}t + e^{\alpha z}\int_\xi^\infty e^{-\beta t}\mathrm{Ai}(t)\mathrm{d}t}{\int_0^\infty e^{-\beta t}\mathrm{Ai}(t)\mathrm{d}t}\right\}. \tag{73}$$

5. Interfacial pressure perturbations

5.1. The long wavelength (small α) limit

The perturbed interfacial pressure can be calculated by first considering the full perturbed vertical momentum equation

$$(D^2 + D - \alpha^2)w_1 = -Dp_1 + \epsilon^{-1}(1 - e^{-z})w_1.$$

The expression shows that to first order the interfacial pressure can be calculated as

$$p_s = -\epsilon^{-1}\int_0^\infty (1 - e^{-z})w_1\mathrm{d}z. \tag{74}$$

Because the perturbed pressure at the mush–liquid interface is given by the convolution of the steady-state velocity profile and the perturbed velocity profile, as shown by Benjamin [19], an approximate interfacial pressure perturbation can be found by integrating over the outer solution. Furthermore, examination of the outer solutions $\tilde{w}_{1+2}^{(0)}$ and $\tilde{w}_3^{(0)}$ reveals that $\tilde{w}_3^{(0)}$ decays much more rapidly away from the origin than does $\tilde{w}_{1+2}^{(0)}$. Therefore, the
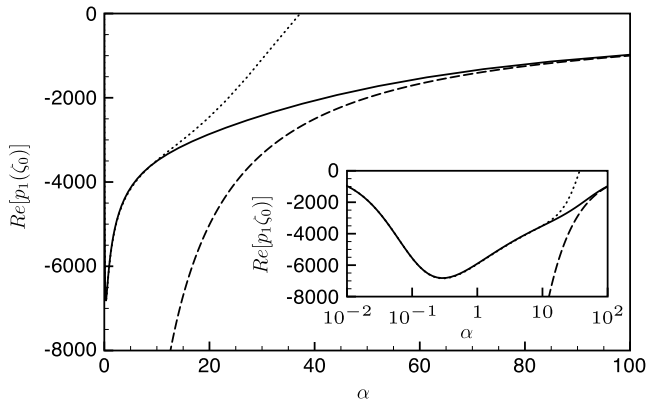
Fig. 4. Comparison of the Frobenius and matched asymptotic derivations of the interfacial pressure perturbation for $U_\infty = 1000$, $Pr = 10$. Here the full Frobenius series solution is plotted (solid) and compared against the asymptotic solution in the small wavelength (dotted) and large wavelength (dashed) limits. The inset is a semilog version of the plot.

pressure perturbation is well approximated by

$$p_s(\alpha) \simeq -\frac{\epsilon^{-1}}{Pr^2} \int_0^\infty (1 - e^{-z}) \frac{\tilde{w}_{1+2}^{(0)}(z)}{\tilde{w}_{1+2}'(0) - \tilde{w}_{1+2}(0)\tilde{w}_3'(0)/\tilde{w}_3(0)} dz.$$

Moreover, the z-dependent component of the integral of $(1 - e^{-z})\tilde{w}_{1+2}^{(0)}$ can be approximated as

$$\int_0^\infty (1 - e^{-z}) e^{-\alpha z} {}_2F_1(p, q, 1 + p + q; e^{-z}) dz$$

$$= \int_0^\infty (1 - e^{-z}) \sum_{n=0}^\infty \frac{(p)_n (q)_n}{(1 + p + q)_n} \frac{e^{-(\alpha+n)z}}{n!} dz$$

$$= \sum_{n=0}^\infty \frac{(p)_n (q)_n}{(1 + p + q)_n} \frac{1}{n!} \int_0^\infty \left[e^{-(\alpha+n)z} - e^{-(\alpha+n+1)z} \right] dz$$

$$= \sum_{n=0}^\infty \frac{(p)_n (q)_n}{(1 + p + q)_n} \frac{1}{n!} \frac{1}{(\alpha + n)(\alpha + n + 1)}.$$

Therefore, we arrive at an excellent approximation of the interfacial pressure perturbation as

$$p_s(\alpha) = -\frac{\alpha^2 U_\infty^2}{Pr} \frac{{}_2F_1(p, q, 1 + p + q; 1)^{-1}}{\tilde{w}_{1+2}'(0) - \tilde{w}_{1+2}(0)\frac{\tilde{w}_3'(0)}{\tilde{w}_3(0)}}$$

$$\times \sum_{n=0}^\infty \frac{(p)_n (q)_n}{(1 + p + q)_n} \frac{1}{n!} \frac{1}{(\alpha + n)(\alpha + n + 1)}. \tag{75}$$

A comparison of the Frobenius series method and this large wavelength (small α) asymptotic result is shown in Fig. 4.

5.2. The short wavelength (large α) limit

The interfacial pressure perturbation can be determined in the large α limit through integration over the fluid layer in a manner identical to the small α limit. In so doing, we write

$$p_s = \epsilon^{-1} \int_0^\infty (1 - e^{-z}) w_1(z) dz$$

$$= \frac{\epsilon^{-2}}{\alpha Pr} \frac{1}{\alpha^2 - 1} \left\{ 1 + \frac{\int_0^\infty e^{-\epsilon^{1/3}\xi} Ai(\xi) d\xi}{\int_0^\infty e^{-\beta\xi} Ai(\xi) d\xi} \right\}, \tag{76}$$

which, in the limit of large α, can be further simplified to

$$p_s \simeq -\frac{U_\infty^2}{\alpha Pr}. \tag{77}$$

The comparison between the Frobenius series method of calculating the pressure perturbation, and the expressions for both the large and small wavenumber limits are shown in Fig. 4 and clearly demonstrate the appropriate asymptotic behavior.

6. Reduced model of the mushy layer: large composition ratio

Now we describe a reduced mushy layer model in which solidification, and the intrinsic interstitial buoyancy, are coupled to the external flow through a pressure matching condition at the mush–liquid interface. The mushy layer is treated using the equations of Section 2. In the absence of an external shear flow it is known that the mushy layer is susceptible to a convective instability driven by the buoyancy of the interstitial fluid [15]. This so-called *mushy layer mode* of convection has streamlines reminiscent of buoyancy driven convection within a porous medium, yet has as its result the dissolution and solidification of the mushy layer in regions of vertical flow. Thus, convection within the mushy layer produces a localized pattern of flow dominated by the formation of chimneys – regions of zero solid fraction – within the mushy layer.

The issue addressed using the simplified approach is how the external fluid flow over the corrugated mush–liquid interface can force convective modes. Such forced convective modes have been explored by Neufeld and Wettlaufer [13] who performed a laboratory study of aqueous ammonium chloride mushy layers. This common saline solution can be solidified at room temperature which, in addition to its ease of handling, has made it a model laboratory system through which one can test the predictions of mushy layer theory. For the present purposes, we use the physical parameters of the ammonium chloride system to motivate a further approximation in our modeling of the forced modes of convection. We note that the relevant values for the laboratory experiments reported in [13] are $\mathcal{C} \simeq 10.2$, $\mathcal{S} \simeq 3.6$, $\theta_\infty \simeq 0.18$. Thus, an analytical solution can be constructed under the assumption of large composition ratio

$$\mathcal{C} \gg |\theta_0|,$$

where $\theta_0 \leq 0$ is the steady-state thermal profile within the mushy layer. This analytic solution was first reported in Feltham and Worster [11] and is used here with the asymptotic pressure solution to provide an analytic model of forced mushy layer convection.

We consider perturbations to the basic state of the form

$$(\theta^m, \phi, u^m, w^m) = (\theta_0^m, \phi_0, u_0^m, w_0^m)$$

$$+ (\theta_1^m, \phi_1, u_1^m, w_1^m) e^{i(k_x x + k_z z)}. \tag{78}$$

In the limit $\mathcal{C} \gg 1$, the equations governing perturbations in the mushy layer can be reduced to

$$\mathcal{C}D\phi_1 + D\theta_1^m = w_1^m D\theta_0^m \tag{79}$$

and $$(D^2 + D - k^2)\theta_1^m = \mathcal{S}D\phi_1 + w_1^m D\theta_0^m, \tag{80}$$

which can be combined to give

$$(D^2 + \Lambda D - k^2)\theta_1^m = \Lambda w_1^m D\theta_0^m. \tag{81}$$

Furthermore, we have shown that in the presence of vigorous external flows the porous medium Rayleigh number is negligible. The perturbed vertical velocity which is decoupled from the thermal field and solid fraction is governed by

$$(D^2 - k^2)w_1^m = 0. \tag{82}$$

The imposition of no normal flow, $w_1^m(0) = 0$, at $z = 0$ where the temperature is eutectic provides the solution of (82),

$$w_1^m(z) = B\sinh(kz). \tag{83}$$

Thus, the general solution to the perturbed thermal field in the mush is

$\theta_1^m(z)$

$$= \frac{e^{-\Lambda z/2}[C \sinh(\gamma z/2) + E \cosh(\gamma z/2)] - \frac{B\theta_\infty}{k\Lambda} e^{-\Lambda(z-\zeta_0)} \cosh(kz)}{F}, (84)$$

where B, C, E and F are all constants to be found by applying the boundary conditions at the mush–liquid interface which are

$$\theta_1^m + \zeta_1 D\theta_0^m = 0, \tag{85}$$

$$\phi_1 + \zeta_1 D\phi_0 = 0, \tag{86}$$

$$D\theta_1^m + \zeta_1 D^2\theta_0^m = 0, \tag{87}$$

$$\text{and} \quad [p]_l^m = 0, \tag{88}$$

where (88) can be rewritten as

$$Dw_1^m = -k^2 \Pi_0 p_s. \tag{89}$$

Using these boundary conditions we find that

$$B = -k\Lambda\theta_\infty^2 \left[\gamma \cosh\left(\frac{\gamma\zeta_0}{2}\right) + \Lambda \sinh\left(\frac{\gamma\zeta_0}{2}\right) \right] \sqrt{1 + \frac{\Lambda}{\theta_\infty}},$$

$$C = \theta_\infty(\Lambda + \theta_\infty) \left[-2k \sinh(k\zeta_0) + \left\{ \Lambda \cosh\left(\frac{\gamma\zeta_0}{2}\right) \right. \right.$$
$$\left. \left. + \gamma \sinh\left(\frac{\gamma\zeta_0}{2}\right) \right\} \sqrt{1 + \frac{\Lambda}{\theta_\infty}} \right],$$

$$E = -\theta_\infty(\Lambda + \theta_\infty) \left[\gamma \cosh\left(\frac{\gamma\zeta_0}{2}\right) \right.$$
$$\left. + \Lambda \sinh\left(\frac{\gamma\zeta_0}{2}\right) \right] \sqrt{1 + \frac{\Lambda}{\theta_\infty}}, \quad \text{and}$$

$$F = \gamma\Lambda + \theta_\infty \left[\gamma + 2k \sinh(k\zeta_0) \sinh\left(\frac{\gamma\zeta_0}{2}\right) \sqrt{1 + \frac{\Lambda}{\theta_\infty}} \right.$$
$$\left. - \cosh(k\zeta_0) \left\{ \gamma \cosh\left(\frac{\gamma\zeta_0}{2}\right) + \Lambda \sinh\left(\frac{\gamma\zeta_0}{2}\right) \right\} \sqrt{1 + \frac{\Lambda}{\theta_\infty}} \right].$$

The base state thermal field and solid fraction of the mushy layer are plotted in Fig. 5a. As discussed previously, perturbations to the mush–liquid interface lead to a Bernoulli suction effect, drawing fluid vertically through the mushy layer under protrusions of the mush–liquid interface. This fluid motion internal to the mushy layer results in a concomitant cooling below the peaks, and dissolution of the crystal matrix as shown in Fig. 5b. The onset of the forced convective pattern at a given external flow speed can be characterized in terms of a porous medium Rayleigh number. In Fig. 6 we show a representative marginal stability curve demarcating the boundary between regimes which are stable (below the curve) and unstable to the forced convective mode. Clearly, for an interfacial perturbation of any wavelength, an increase in the permeability increases the ease with which flow can be driven in the mushy layer, thereby facilitating the generation of a forced convective mode.

The stability of this reduced model system is shown in Fig. 7 by plotting the critical Rayleigh number R_m^c, as a function of the external flow U_∞, for various Darcy numbers Π_0. We observe that for small U_∞ stability is dominated by the buoyant mushy layer mode of convection, which is independent of the Darcy number. As the external shear flow is increased, the forced mushy layer mode becomes dominant, first for the most permeable mushy layers (large Π_0) and eventually for less permeable mushy layers (smaller Π_0). This dependence on the permeability is due to the importance
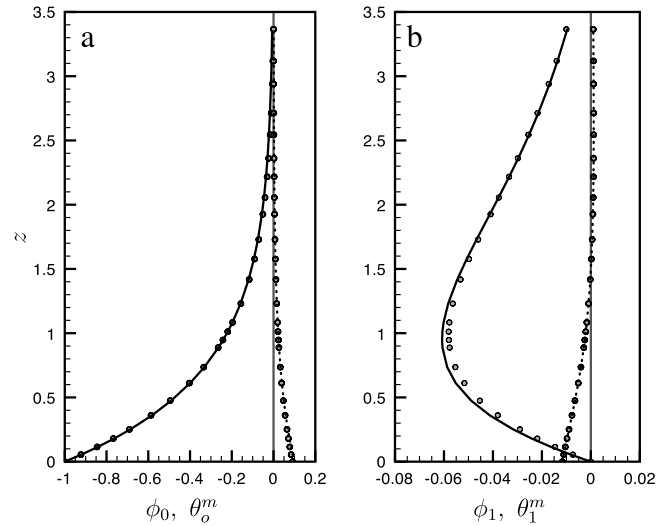

Fig. 5. The base state thermal field (solid) and solid fraction (dotted) are plotted in (a) for $\mathcal{C} = 10$, $\mathcal{S} = 5$ and $\theta_\infty = 0.01$ and are compared to the full numerical solution of [13] (circles). The system is forced with pressure perturbations at the mush–liquid interface for $U_\infty = 100$ and $Pr = 10$. The perturbed thermal field (solid) and solid fraction (dotted) are plotted in (b) for the same parameter values and again the full numerical solution is given by the circles.
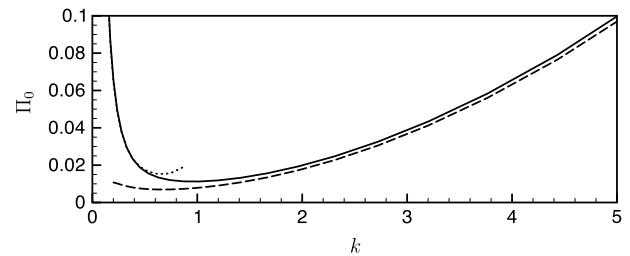

Fig. 6. Marginal stability curve in which the dimensionless permeability, or Darcy number Π_0 is plotted versus the wavenumber, k, for $U_\infty = 100$ and $Pr = 10$. Above the curve the system is unstable to the forced convective mode. The marginal stability curve shown is produced using the pressure perturbation derived using the Frobenius method (solid), the short (dashed) and long (dotted) wavelength matched asymptotic results. The experimental parameters are $\mathcal{C} = 10.2$, $\mathcal{S} = 3.6$ and $\theta_\infty = 0.2$ [13].
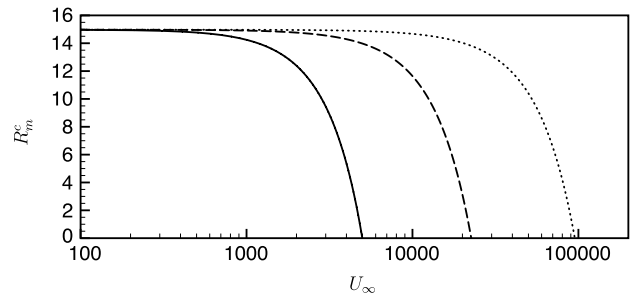

Fig. 7. The critical porous medium Rayleigh number is plotted as a function of the external flow rate for Darcy numbers $\Pi_0 = 10^{-3}$ (solid), 10^{-4} (dashed) and 10^{-5} (dotted).

of permeability in coupling pressure perturbations in the outer liquid to flow within the mushy layer as clearly seen in the pressure matching boundary condition (89).

To summarize, solutions to the approximate perturbation equations are found in the mushy layer, forced by pressure perturbations at the mush–liquid interface. These pressure perturbations are found using both a Frobenius series method and analytically by the method of matched asymptotic expansions in the short and long wavelength limits. Thus, solutions for the perturbed velocity,

temperature and solid fraction in the mushy layer can therefore be obtained analytically in the limit $\mathcal{C} \gg 1$ and $\theta_\infty \simeq 0$.

7. Discussion and conclusion

Flows involving a change of phase are amongst a class of problems that capture the interest of a broad range of scientists and engineers. One such circumstance involves the interaction between natural and forced flows with the solidification of multicomponent solutions. A quantitative understanding of these systems is sought through many different experimental, numerical and analytical means. The setting combines a number of classical issues in moving boundary problems with the singular perturbations that arise in the analysis of hydrodynamic boundary layers, but here with the additional influence of a permeable and chemically reactive "wall". In the case we have studied, in which an external shear flow is imposed upon a growing mushy layer, our first approach was a combined experimental and hybrid numerical–theoretical analysis [10,13]. In this paper we provide a detailed physical picture of the system through an asymptotic analysis of how regions within the mushy layer and fluid boundary layer interact with the far-field flow. The value of this approach is that it highlights the key physical balances that operate when solidifying fluids interact with fluid flows.

Our approach was to decompose the problem into an analysis of the forced dissolution and solidification of a mushy layer coupled to, and driven by, interactions with the external fluid flow via a corrugated mush–liquid interface. This separation was made possible through the realization that in most experimental systems the Darcy permeability is small and thus, to leading order, flow within the liquid impinges upon an impermeable boundary. In consequence, the pressure at the mush–liquid interface available to drive interstitial flow and concomitant phase change was calculated by matching the outer inviscid flow to the inner viscous sublayer. As observed experimentally [13], this interstitial flow created by the pressure perturbation alters the spatiotemporal dendritic structure of the mushy layer and leads to a regular pattern of dissolution and solidification transverse to the flow direction. For the case of large Stefan number, we were able to derive an analytical expression for the critical porous medium Rayleigh number driving this process. These results compare well with numerical solutions and thereby provide an accessible and quantitatively reliable framework for researchers interested in many different applications. Finally, because of the degree of difficulty of a numerical approach to such problems, the development of a solely analytical framework provides the necessary basis from which one can pursue a host of related problems. Among those of industrial and geophysical importance is the solidification of anisotropic crystalline mushy layers and the inherent possibility of manipulating materials properties through the application of an external flow.

Acknowledgements

References

[1] M.G. Worster, Solidification of fluids, in: Perspectives in Fluid Dynamics: A Collective Introduction to Current Research, Cambridge University Press, 2000, pp. 393–446 (Chapter).

[2] D.L. Feltham, N. Untersteiner, J.S. Wettlaufer, M.G. Worster, Sea ice is a mushy layer, Geophys. Res. Lett. 33 (2006) L14501. doi:10.1029/2006GL026290.

[3] X. Song, Anisotropy of the earth's inner core, Rev. Geophys. 35 (1) (1997) 297–313.

[4] S.H. Davis, Theory of Solidification, Cambridge University Press, Cambridge, 2001, p. 385.

[5] K. Widell, I. Fer, P.M. Haugan, Salt release from warming sea ice, Geophys. Res. Lett. 33 (2006) L12501. doi:10.1029/2006GL026262.

[6] M.G. McPhee, Air-Ice-Ocean Interaction: Turbulent Ocean Boundary Layer Exchange Processes, Springer, New York, 2008, p. 215.

[7] W.F. Weeks, On Sea Ice, University of Alaska Press, Fairbanks, 2010, p. 680.

[8] R.R. Gilpin, T. Hirata, K.C. Cheng, Wave formation and heat transfer at an ice–water interface in the presence of a turbulent flow, J. Fluid Mech. 99 (1980) 619–640.

[9] J.S. Wettlaufer, Heat flux and the ice–ocean interface, J. Geophys. Res. 96 (1991) 7215–7236.

[10] J.A. Neufeld, J.S. Wettlaufer, Shear-enhanced convection in a mushy layer, J. Fluid Mech. 612 (2008) 339–361.

[11] D.L. Feltham, M.G. Worster, Flow-induced morphological instability of a mushy layer, J. Fluid Mech. 391 (1999) 337–357.

[12] J.A. Neufeld, J.S. Wettlaufer, D.L. Feltham, M.G. Worster, Corrigendum to flow-induced morphological instability of a mushy layer, J. Fluid Mech. 549 (2006) 442–443.

[13] J.A. Neufeld, J.S. Wettlaufer, An experimental study of shear-enhanced convection in a mushy layer, J. Fluid Mech. 612 (2008) 363–385.

[14] P.G. Drazin, W.H. Reid, Hydrodynamic stability, in: Cambridge Monographs on Mechanics and Applied Mathematics, Cambridge University Press, 1981.

[15] M.G. Worster, Instabilities of the liquid and mushy regions during solidification of alloys, J. Fluid Mech. 237 (1992) 649–669.

[16] H.E. Huppert, M.G. Worster, Dynamic solidification of a binary melt, Nature 314 (1985) 703–707.

[17] M.G. Worster, Solidification of an alloy from a cooled boundary, J. Fluid Mech. 167 (1986) 481–501.

[18] G.S. Beavers, D.D. Joseph, Boundary conditions at a naturally permeable wall, J. Fluid Mech. 30 (1) (1967) 197–207.

[19] T.B. Benjamin, Shearing flow over a wavy boundary, J. Fluid Mech. 6 (1959) 161–205.

[20] F. Charru, E.J. Hinch, 'Phase diagram' of interfacial instabilities in a two-layer couette flow and mechanism of the long-wave instability, J. Fluid Mech. 414 (2000) 195–223.

[21] F. Charru, E.J. Hinch, Ripple formation on a particle bed sheared by a viscous liquid. part 1. steady flow, J. Fluid Mech. 550 (2006) 111–121.

[22] W.H. Reid, The stability of parallel flows, in: Basic Developments in Fluid Dynamics, vol. 1, Academic Press, 1965, pp. 249–307.

[23] T.H. Hughes, W.H. Reid, On the stability of the asymptotic suction boundary-layer profile, J. Fluid Mech. 23 (4) (1965) 715–735.

[24] L.M. Hocking, Non-linear instability of the asymptotic suction velocity profile, Quart. J. Mech. Appl. Math. 28 (3) (1975) 341–353.

[25] W.D. Lakin, W.H. Reid, Asymptotic analysis of the Orr–Sommerfeld problem for boundary-layer flows, Quart. Mech. Appl. Math. 35 (1) (1982) 69–89.

[26] C.M. Bender, S.A. Orszag, Advanced Mathematical Methods for Scientists and Engineers: Asymptotic Methods and Perturbation Theory, Springer-Verlag, New York, 1991.

[27] W. Tollmien, Über die entstehung der turbulenz, Nachrichten der Gesellschaft der Wissenschaften zu Göttingen, Mathematisch-Phys. Klasse (1929) 21–44.

[28] M. Abramowitz, I.A. Stegun (Eds.), Handbook of Mathematical Functions with Formulas, Graphs and Mathematical Tables, 10th ed., Dover Publications Inc., 1972.

[29] M. Van Dyke, Perturbation Methods in Fluid Mechanics, The Parabolic Press, Stanford, California, 1975.